Monitoring microstructural evolution in-situ during cyclic deformation by high resolution reciprocal space mapping

2017 J. Phys.: Conf. Ser. 843 012031

(http://iopscience.iop.org/1742-6596/843/1/012031)

IOP Conf. Series: Journal of Physics: Conf. Series **843** (2017) 012031 doi:10.1088/1742-6596/843/1/012031

Monitoring microstructural evolution in-situ during cyclic deformation by high resolution reciprocal space mapping

Annika M. Diederichs[*1], Felix Thiel[1,2], Torben Fischer[3], Ulrich Lienert[4], Wolfgang Pantleon[1]

1: Department of Mechanical Engineering, Materials and Surface Engineering, Technical University of Denmark, 2800 Kgs. Lyngby, Denmark.

2: Institute for Metallic Materials, Leibniz Institute for Solid State and Materials Research, 01690 Dresden, Germany.

3: Helmholtz-Zentrum Geesthacht, Institute of Materials Research, 21502 Geesthacht, Germany.

4: DESY Photon Science, Deutsches Elektronen-Synchrotron, 22607 Hamburg, Germany.

*anmad@mek.dtu.dk

Abstract. The recently developed synchrotron technique High Resolution Reciprocal Space Mapping (HRRSM) is used to characterize the deformation structures evolving during cyclic deformation of commercially pure, polycrystalline aluminium AA1050. Insight into the structural reorganization within single grains is gained by in-situ monitoring of the microstructural evolution during cyclic deformation. By HRRSM, a large number of individual subgrains can be resolved within individual grains in the bulk of polycrystalline specimens and their fate, their individual orientation and elastic stresses, tracked during different loading regimes as tension and compression. With this technique, the evolution of dislocation structures in selected grains was followed during an individual load cycle.

1. Introduction

Fatigue-related damage due to repeatedly changing mechanical loading is one of the major failure reasons in structural materials. During mechanical loading of metals, plastic deformation occurs by motion of dislocations causing dislocations to be stored in the material [1]. For an understanding of the materials response to repeated mechanical loading, it is central to understand the interaction between these dislocations. While final failure occurs on the macroscale, changing mechanical loads cause on the micro- and nanoscale formation of characteristic dislocation structures, which play a decisive role for the materials life time.

During cyclic deformation of face-centered cubic metals with high stacking fault energy such as aluminium, dislocations self-organize into ordered structures, consisting of dislocation walls of high dislocation density separating almost dislocation-free subgrains with dimensions of 2-5 μm [2-7]. Their specific morphology is influenced by the deformation conditions such as the strain (or stress) amplitude, the strain rate and the number of cycles during cyclic deformation, where higher strain amplitudes causes

an earlier onset of structure formation and larger misorientations [7-12]. The internal dislocation structure influences the lifetime of the material during cyclic deformation, because different mechanical properties are associated with dislocation walls and subgrains as rationalized in the composite model [13-14]. Subgrains yield more easily (at lower stresses) than dislocation walls and intergranular stresses arise to ensure compatible deformation. Information about internal strains can be gained from local changes of the lattice parameter, which can be determined by X-ray diffraction [13]. The characteristic dislocation structures are known to determine the plastic deformation behavior and thus the flow stress, but the mechanisms on the microscale are still insufficiently understood and their relation to macroscopic failure unsettled, because of limitations in the characterization techniques available.

Traditionally, dislocation structures were studied with classical X-ray line profile analysis using conventional X-ray diffractometers [15], but recently synchrotron-based techniques were developed as tools for non-destructive microscale characterization of bulk samples [16-18]. Due to their large penetration depth, high energy X-rays are suitable for non-destructive investigations on macroscopic specimens. While the signal in classical analysis originates from many different grains with different orientations, individual diffraction peaks of single grains can be selected by High Resolution Reciprocal Space Mapping (HRRSM) and the intensity distribution of a diffraction peak mapped in reciprocal space with high resolution ($\Delta q = 5 \cdot 10^{-4}$ Å^{-1} [16]). In this manner, structural features within individual grains can be identified due to their slightly different and unique orientations. By purposely designed load frames, metallic specimens can be deformed in-situ and, hence, the microstructural evolution in single grains followed during changing mechanical loads [16-17].

The feasibility of high resolution reciprocal space mapping has been demonstrated and successfully applied to in-situ tensile testing, loading/unloading sequences and strain path changes [14,16-17,19-24]. The aim of the present study is to gain insight into cyclic deformation by applying HRRSM to monitor individual grains in commercially pure, polycrystalline aluminium AA1050 bulk samples in-situ during a tension/compression sequence.

2. Test specimen

Tensile test specimens were manufactured by spark cutting from an AA1050 sheet cold-rolled to 90% thickness reduction to a final thickness of 1 mm. The geometry of the dog bone-shaped specimens (with a gauge section of 15 mm in length and 5 mm in width) is shown in Figure 1. The tensile specimens were annealed at 600 °C for 2 h to ensure homogeneous recrystallization. The microstructure after annealing was investigated metallographically to confirm homogeneous recrystallization throughout the entire gauge section of the specimen. Grain sizes were estimated to be between 30 µm and 100 µm using both, light optical microscopy and scanning electron microscopy in particular Electron Backscatter Diffraction and Electron Channeling Contrast Imaging.

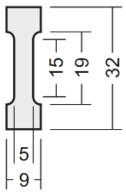

Figure 1. Geometry of dog bone-shaped tensile specimen manufactured from a cold-rolled AA1050 sheet (thickness 1 mm) for cyclic testing (lengths are in mm).

The tensile specimens were pre-fatigued using an MTS Acumen 3 kN Electrodynamic Test System equipped with Station Manager MTS FlexTest 40 and pneumatic grips. Cyclic pre-deformation was carried out in order to introduce a microstructure conform to cyclic deformation (and potentially giving rise to fatigue failure) in the specimen prior to the in-situ investigations by HRRSM. The sample was initially deformed by tension to a strain of 2% with a grip speed of 0.015 mm/s. Afterwards, displacement-controlled tension-compression cycling was performed with a rate of 0.5 Hz and a

displacement amplitude of 20 μm corresponding to a nominal strain amplitude of $\hat{\varepsilon} = 1.3 \cdot 10^{-3}$. Cyclic deformation was stopped after 44350 cycles at the end of the compression half cycle and unloaded. At this stage, no significant changes of the maximal tensile and compressive stresses were recorded during cyclic testing.

3. High Resolution Reciprocal Space Mapping (HRRSM)

The experiment was carried out at beam line P07 at PETRA III with a monochromatic beam of 53 keV. HRRSM was performed in-situ while loading the pre-fatigued sample using the custom-made load frame shown in Figure 2a. The setup was essentially similar to an earlier setup at APS [16-17] developed to obtain three-dimensional reciprocal space maps with high resolution to monitor individual bulk grains during deformation of polycrystalline samples. A sketch of the modified setup used in the experimental hutch EH3 at P07 is presented in Figure 2b.

An unloaded, pre-fatigued sample was equipped with two HBM LY4 standard strain gauges (glued on the opposite sides of the specimen, aligned with the tensile axis and centered with respect to gauge section) to monitor the strain in-situ and to reveal potential specimen bending. The sample was mounted in a transportable screw-driven load frame equipped with a 5 kN load cell. Both strain and axial force were monitored during mounting, deformation and dismounting of the sample. The load frame with the sample was placed with the load axis horizontally on a *xy* translation stage on top of a rotation stage allowing rotation of the entire load frame around the vertical *z* axis. Translation along *z* could be achieved by the heavy duty hexapod in EH3. The beam was focused in vertical direction to a Gaussian width of 10 μm and narrowed in horizontal direction to 50 μm allowing complete illumination of individual grains with sizes up to 30 μm. Grains are selected with the help of a Perkin Elmer XRD 1621 xN detector placed 70 cm behind the sample on a horizontal translation by finding isolated 400 diffraction peaks not overlapping with peaks of other grains. After identifying suitable grains, the near detector is moved out of the beam and the diffraction peaks are investigated by a MarCCD165 placed 3.9 m behind the sample on the location of a 400 diffraction peak with diffraction vector close to the tensile axis, i.e. in the horizontal diffraction plane at a diffraction angle $2\theta_{400}$ of 13.63° for aluminium.

An entire sequence of two-dimensional images of the 400 diffraction peak are acquired with the distant detector, while rocking the sample around the vertical axis perpendicular to the scattering plane in small intervals of the rocking angle ω. By stacking the images recorded for several adjacent ω intervals, three-dimensional distributions (two directions on the detector and the additional rocking) of the diffracted intensity are obtained representing three-dimensional reciprocal space maps. The desired high resolution is determined by the monochromaticity and divergence of the beam, the point spread function of the detector as well as by the chosen angular intervals of the rocking (for the presented data, the latter being 0.015° corresponding to $2 \cdot 10^{-3}$ Å^{-1}).

Three-dimensional reciprocal space maps can be assessed in two complementary projections: azimuthal projections and radial peak profiles, which represent the distributions of lattice plane inclinations and normal strains, respectively. As the crystalline lattice within individual grains becomes locally distorted by dislocation structures with subgrains separated by dislocation walls, the intensity distributions of individual diffraction peaks are not completely smooth. Two components can be distinguished [16,19], where sharp peaks of high intensity correspond to individual subgrains and a smooth cloud of lower intensity results from dislocations walls. By separating the two contributions numerically [22], intensity distributions corresponding to individual subgrains can be identified and analyzed individually for all load steps.

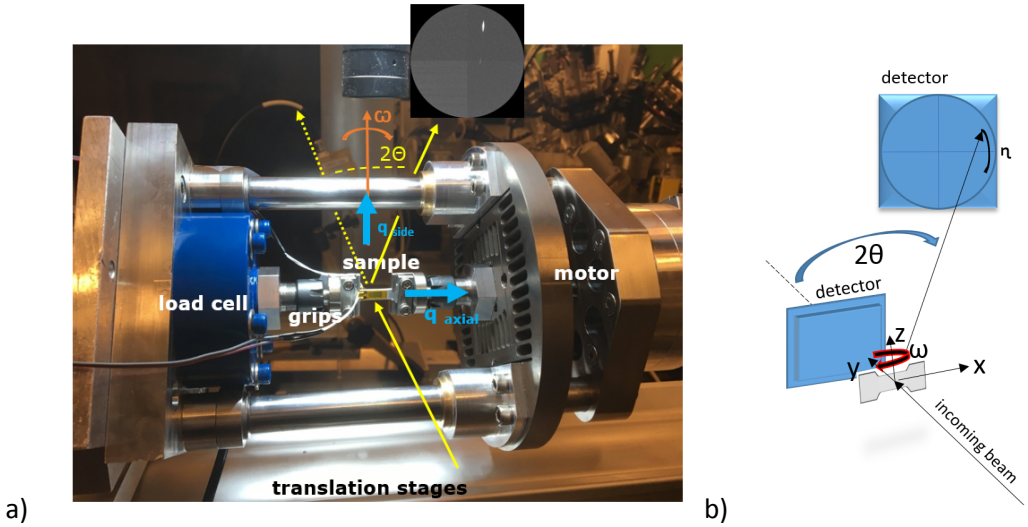

a) b)

Figure 2. a) Load frame (from P21 at PETRA III) used for tensile and compressive deformation in-situ during High Resolution Reciprocal Space Mapping. A dog bone-shaped sample (with two strain gauges) is mounted in the load frame and loaded in horizontal direction by a screw-driven motor. The load frame is positioned on translation stages on top of a fast rotation stage with rotation axis perpendicular to the scattering plane (i.e. allowing rocking in ω). b) Sketch of the HRRSM set-up in EH3 at P07. The near detector is used for finding suitable grains and will be moved out of the beam path for reciprocal space mapping. The latter is achieved by acquisition of intensity distributions of the 400 diffraction peak from a selected grain with the distant detector during rocking of the sample using the ω rotation.

4. Experimental results

The aim of the experiment was to follow changes in the deformation structure of selected grains (having a ⟨400⟩ direction parallel to the tensile axis) during a tensile/compression sequence (or in terms of cyclic deformation: during an individual load cycle). By using the pre-fatigued specimen unloaded from maximum compression, an incomplete load cycle (cf. Figure 3) was achieved by following the hysteresis curve to maximal tensile load and continuing into compression to a relevant load. For obtaining reciprocal space maps, the deformation was paused at selected forces:

Since the pre-deformation was stopped at the highest compressive load in the hysteresis curve, it was aimed for characterizing the deformation structure after loading the sample with a load as small as permissible to hold the specimen tight (almost 0 N, L0). The tensile loading was interrupted and kept at the force for a first time at 70 N (L1) to analyze the behavior during elastic loading. For the following mapping (at 100 N, L2), the deformation was paused after a significant change in strain. Next, the tensile loading was stopped at the maximum force of 140 N (L3) corresponding to the highest tensile load the sample experienced during cyclic pre-deformation. During unloading along the hysteresis curve to 60 N (U1) only small changes in strain were observed, whereas at a compressive load of -100 N (U2), which is slightly below the highest compressive force during pre-deformation, a significant compressive strain was attained. For halting the deformation manually when reaching the desired loads, a slow grip speed of 0.003 mm/s was chosen. By utilizing two strain gauges at the opposite sides of the specimen, bending during compression can be detected. Such bending has been observed for similarly pre-fatigued specimens when exceeding compressive loads of -180 N corresponding to the theoretical buckling stress. Due to the low material strength, a slight bending occurred when mounting the specimen in the grips leading to internal stresses and strains in the specimen.

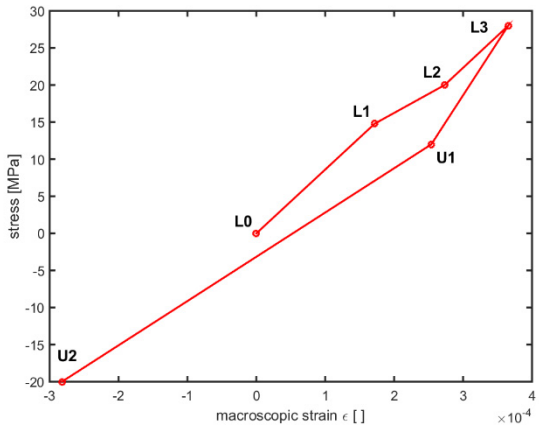

Figure 3. Hysteresis curve showing the incomplete load cycle performed in-situ. Reciprocal space maps were obtained at the designated points (L0-3, U1-2) while pausing the deformation for HRRSM. The maximal force of 140 N corresponds to the maximal tensile force during the cyclic pre-deformation of the sample (due to time limitations, no data were recorded at the maximal compressive force of -140 N).

At each of the load steps where the deformation was paused, reciprocal space maps of six different grains were collected; all having a ⟨400⟩ direction close to the tensile axis. The overall behavior of all grains is similar and only exemplary data are presented. Figure 4 shows the azimuthal projection, a projection of the intensity distribution in reciprocal space parallel to the diffraction vector, representing the different inclination of the (400) planes in grain A for the initial configuration (load step L0). Such maps form the basis for an identification of individual subgrains by their diffraction signature – the high-intensity peaks. Up to 100 high-intensity peaks corresponding to 100 individual subgrains were identified in each reciprocal space map. One high-intensity peak corresponding to a subgrain of grain A, which could be identified in the azimuthal projections of all load steps, is highlighted in Figure 4 and selected for exemplary analysis.

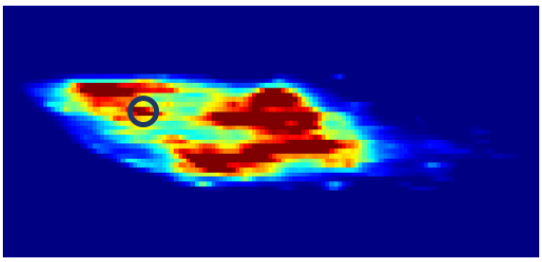

Figure 4. Azimuthal projection (with η horizontally covering a range of 0.3° and the rocking angle ω vertically covering a range of 1.2°) of the 400 diffraction peak from grain A before any significant tensile loading (L0). The intensity distribution is not smooth and one obvious high-intensity peak corresponding to a single subgrain is marked by a black circle.

Figure 5a shows radial peak profiles, which are projections of the reciprocal space maps on the direction of the diffraction vector, for grain A for all different loading steps. The radial position can be characterized either by the diffraction angle 2θ (from Bragg's equation $2d_{400}\sin\theta = \lambda$ with the wave length λ of the used X-rays and the lattice plane spacing d_{400}) or by the amount of the diffraction vector

$$q = \frac{4\pi}{\lambda}\sin\theta\,. \qquad (1)$$

The obtained radial profiles can be further analyzed regarding their position, width and asymmetry and provide information on the lattice strain along the diffraction vector. The peak position can be quantified by the average position $q_{mean} = 2\pi/d_{400}$ which is inversely proportional to the lattice plane spacing. As seen from Figure 5a, the peak position changes to smaller values during tensile loading (L1-3), due to increasing elastic strain and increasing lattice plane spacing, and, vice versa, to higher values during unloading and compression (U1-2), due to decreasing or negative strain, respectively, and a smaller lattice plane spacing as a consequence of the elastic deformation caused by the applied load. No significant change in the peak shape is observed and the peak width seems to stay rather constant.

Figure 5b shows the mean peak positions q_{mean} of three different grains for all six different loading steps (i) in dependence of the total macroscopic strain (in colors) measured by the strain gauges and (ii) in dependence of the purely elastic strains (green)

$$\varepsilon = \frac{d - d_0}{d_0} = \frac{q_{mean,\mathrm{L0}}}{q_{mean}} - 1 \qquad (2)$$

calculated from the deviation of the actual peak position from its initial value $q_{mean,L0}$. The peak position behaves similar for all three presented grains and reproduces in general the hysteresis curve of the in-situ experiment (Figure 3). The absolute values of the diffraction vector q_{mean} are surprisingly different from grain to grain and differ by 0.08 Å^{-1} between the three presented grains. Correspondingly, the elastic strain ε calculated from the mean peak position with respect to the presumed strain-free initial value not only differs from the total strain measured by the strain gauges, but also varies from grain to grain. This indicates the presence of large internal elastic stresses within the specimen, most likely caused by the bending through clamping when mounting the sample in the testing machine or in the load frame. Notably, the changes in the calculated elastic strains follow the applied load as expected from Hooke's law with the proper value of Young's modulus for aluminium.

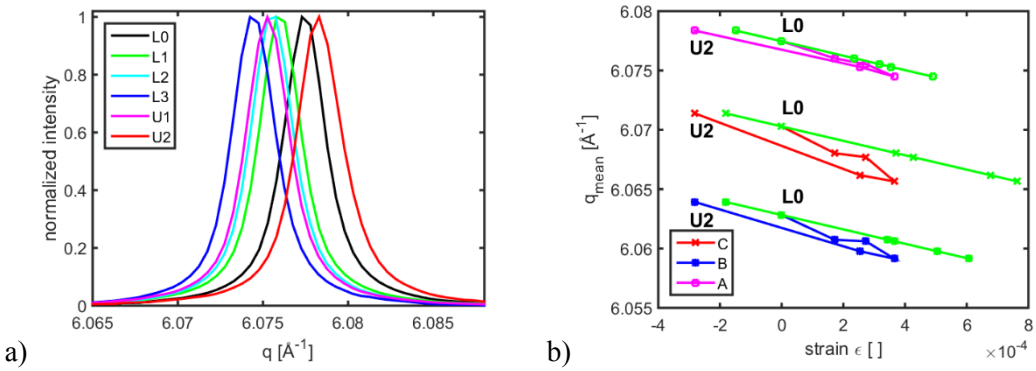

Figure 5. a) Radial peak profiles of grain A for the six different loading steps during tensile and subsequent compressive loading of the pre-fatigued sample. b) Mean peak position of three selected grains as function of the total strain measured by the strain gauges (magenta, red, blue) and the elastic strain (green) calculated from the mean peak position according to equation (2).

Radial peak profiles of subgrains are analyzed in the same way. Figure 6a shows the radial profiles for the single subgrain of grain A marked in Figure 4. This particular subgrain (among others) could be identified for all six load steps by its specific position in the azimuthal projections for grain A. The radial profiles of the subgrain behave similar to the radial profiles observed for the entire grain A. As shown in Figure 6b, the peak position of the particular subgrain shifts to lower values of q during tensile loading and to higher values of q during unloading and compression, while neither peak shape, nor peak width changes significantly.

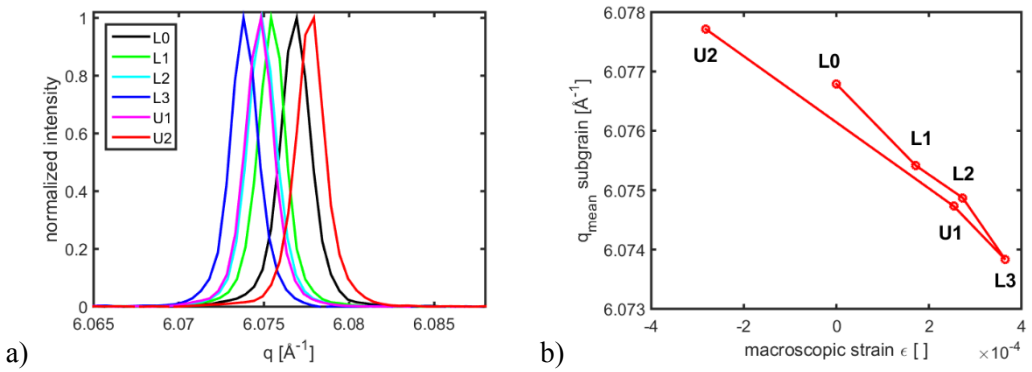

Figure 6. a) Radial peak profiles for the selected subgrain from grain A marked in Figure 4 for all load steps. The profiles shift similar to the profile of the entire grain A. b) Mean peak position of the selected subgrain as a function of the macroscopic total strain for all load steps.

Since up to 100 high-intensity peaks are identified in each reciprocal space map, a statistical analysis of their peak positions can be attempted in addition to the analysis of the fate of individual subgrains. Figure 7 presents a normal probability plot of the peak positions of the 80 largest subgrains. Essentially each subgrain has a different peak position (and hence experiences a different elastic strain); these peak positions are Gaussian distributed for each load step and shift in accordance with the applied load (cf. [14,24]).

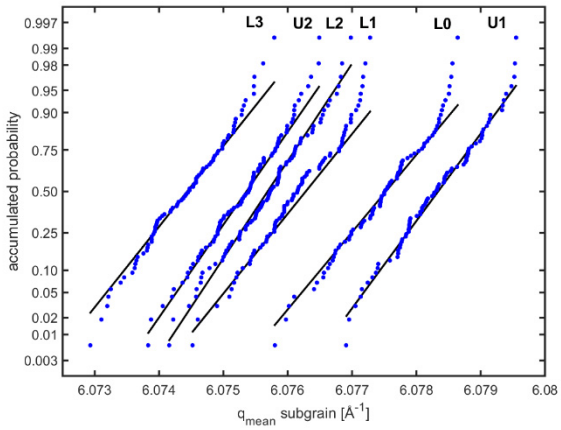

Figure 7. Normal probability plot of the peak positions of the 80 most intense high-intensity peaks corresponding to the 80 largest subgrains of grain A for all six load steps. Best linear fits to the data are shown as black lines indicating that the peak positions of the subgrains follow a Gaussian distribution at each load step.

5. Discussion

From the obtained reciprocal space maps certain features of the dislocation structure within the grains were revealed: High-intensity peaks corresponding to individual subgrains can be identified and separated from smooth intensity distributions using numerical methods [22]. In this manner, the existence of ordered dislocation structures during cyclic deformation is proven in-situ without any need for destructive post-mortem investigations by e.g. electron microscopy. Spatial imaging of the evolving deformation structure in-situ, on the other hand, would require further development of other synchrotron diffraction techniques such as dark field X-ray microscopy [18].

It was observed that the mean peak position q_{mean} of the radial profiles from an individual grain shifts as expected during tensile and compressive loading to lower and higher values of the diffraction vector (cf. Figure 5), respectively, as consequence of purely elastic distortion of the lattice [13-14,24]. While the radial profiles only shift about 0.05 $Å^{-1}$ during the load cycle, a higher difference of 0.08 $Å^{-1}$ is found between the peak positions of different grains. The observed difference between different grains (cf. Figure 5b) is attributed to different internal stresses caused mainly by bending during mounting of the pre-fatigued specimen before any loading took place. As the method is sensitive to local elastic strains, already minor specimen bends can cause the observed effect.

Analysis of the 80 largest subgrains in a selected grain has shown that their radial peak position follow a Gaussian distribution at each step in the load cycle (as revealed earlier for different loading conditions [14,24]). As only minor changes in the overall deformation structure occur during a single load cycle, individual subgrains could be followed in-situ during the (incomplete) load cycle. Their radial profiles show the same characteristics as the radial profile of the entire grain. Nevertheless, we expect to be able to reveal more subtle changes during an individual cycle, by analyzing the behavior of several subgrains individually in more detail and a thorough analysis of their statistical distributions. A hint on such slight changes (which have to be substantiated by findings on other grains) can be gained from the best linear fits in Figure 7 which do not follow exactly the same slope revealing a slight change in their distribution. In the end, there are these small changes which during repeated tension/compression cycles will evolve the deformation structures finally causing fatigue failure. For a complete description of the microstructural changes, the evolution of the microstructure should be followed over a number of load cycles by pausing the cyclic deformation after numerous load cycles.

6. Conclusions

High Resolution Reciprocal Space Mapping was successfully applied to follow the evolution of the deformation structure in several grains (which all had in common a ⟨400⟩ direction close to the loading direction) embedded in a pre-fatigued AA1050 sample in-situ during an individual load cycle, while monitoring stress and strain simultaneously.

The preliminary results show that High Resolution Reciprocal Space Mapping is a promising technique for in-situ investigations of cyclic deformation of metals providing detailed insight in the development of deformation structures during varying loads. In this manner, quantitative information about dislocation structures in individual bulk grains embedded in test specimens can be obtained during individual load cycles.

Acknowledgements

The authors gratefully acknowledge the financial support from MAX4ESSFUN of the European Regional Development Fund Interreg Öresund-Kattegat-Skagerrak (project DTU-007) and DANSCATT. The authors also acknowledge beamtime by DESY under proposal number I-20150204 EC. We would like to thank Dmytro Orlov for his participation and valuable discussions.

References

[1] Laird C, Charsley P and Mughrabi H 1986 Low energy dislocation structures produced by cyclic deformation *Materials Science and Engineerin*g **81** 433-450
[2] Li P, Li S X, Wang Z G and Zhang Z F 2011 Fundamental factors on formation mechanism of dislocation arrangements in cyclically deformed fcc single crystals *Progress Materials Science* **56**(3) 328-377
[3] Nellessen J, Sandlöbes S and Raabe D 2016 Low cycle fatigue in aluminum single and bi-crystals: On the influence of crystal orientation *Materials Science and Engineering A* **668** 166-179
[4] Wang J, Zhu Z G, Fang Q F and Liu G D 1999 The influence of the crystallographic orientation on the behavior of fatigue in Al single crystals *Materials research bulletin* **34**(3) 407-413
[5] Vorren O and Ryum N 1988 Cyclic deformation of Al single crystals: Effect of the crystallographic orientation *Acta Metallurgica* **36**(6) 1443-1453
[6] Xia Y B 1993 The effect of crystal orientation on mechanical behavior during fatigue in aluminium single crystals *Scripta metallurgica et materialia* **29**(7) 999-1003
[7] Snowden K U 1963 Dislocation arrangements during cyclic hardening and softening in A1 crystals *Acta metallurgica* **11**(7) 675-684
[8] Li P, Li S and Wang Z 2010 Cyclic deformation behaviors of [-5 7 9] oriented Al single crystals *Metall. Mater. Transactions A* **41** 2532-2537
[9] Fujii T, Sawatari N, Onaka S and Kato M 2004 Cyclic deformation of pure aluminum single crystals with double-slip orientations *Materials Science and Engineering: A* **387** 486-490
[10] El-Madhoun Y, Mohamed A and Bassim M N 2003 Cyclic stress–strain response and dislocation structures in polycrystalline aluminum *Materials Science and Engineering: A* **359**(1) 220-227
[11] Grosskreutz J C and Waldow P 1963 Substructure and fatigue fracture in aluminum *Acta metallurgica* **11**(7) 717-724
[12] Mitchell A B and Teer D G 1970 The analysis of dislocation structures in fatigued aluminium single crystals exhibiting striations *Philosophical Magazine* **22**(176) 399-417
[13] Mughrabi H 1983 Dislocation wall and cell structures and long-range internal stresses in deformed metal crystals *Acta metallurgica* **31**(9) 1367-1379
[14] Pantleon W, Wejdemann C, Jakobsen B, Lienert U and Poulsen H F 2010 Advances in characterization of deformation structures by high resolution reciprocal space mapping *Proceedings Risø International Symposium on Materials Science* DTU Risø **31** 79-100
[15] Ungár T 2001 Dislocation densities, arrangements and character from X-ray diffraction experiments *Materials Science and Engineering: A* **309** 14-22
[16] Jakobsen B, Poulsen H F, Lienert U, Almer J, Shastri S D, Sørensen H O and Pantleon W 2006 Formation and subdivision of deformation structures during plastic deformation *Science* **312**(5775) 889-892
[17] Pantleon W, Wejdemann C, Jakobsen B, Lienert U and Poulsen H F 2009 Evolution of deformation structures under varying loading conditions followed in situ by high angular resolution 3DXRD *Materials Science and Engineering: A* **524**(1) 55-63
[18] Simons H, King A, Ludwig W, Detlefs C, Pantleon W, Schmidt S, Stöhr F, Snigireva I, Snigirev A and Poulsen H F 2015 Dark-field X-ray microscopy for multiscale structural characterization *Nature communications* NC06(2015)6098
[19] Jakobsen B, Poulsen H F, Lienert U, and Pantleon W 2007 Direct determination of elastic strains and dislocation densities in individual subgrains in deformation structures *Acta materialia* **55** 3241-3430
[20] Pantleon W, Poulsen H F, Almer J and Lienert U 2004 In situ X-ray peak shape analysis of embedded individual grains during plastic deformation of metals *Materials Science and Engineering: A* **387** 339-342
[21] Jakobsen B, Poulsen H F, Lienert U, Bernier J, Gundlach C and Pantleon W 2009 Stability of dislocation structures in copper towards stress relaxation investigated by high angular resolution 3D X-ray diffraction *physica status solidi (a)* **206**(1) 21-30
[22] Wejdemann C, Lienert U, Nielsen H B and Pantleon W 2010 Identifying individual subgrains in evolving deformation structures by high angular resolution X-ray diffraction *Proceedings Risø International Symposium on Materials Science* DTU Risø **31** 477-487
[23] Wejdemann C, Lienert U and Pantleon W 2010 Reversal of asymmetry of X-ray peak profiles from individual grains during a strain path change *Scripta Materialia* **62**(10) 794-797
[24] Wejdemann C, Poulsen H F, Lienert U and Pantleon W 2013 In situ observation of the dislocation structure evolution during a strain path change in copper *JOM* **65**(1) 35-43